Strain Mapping Inkjet-Printed Resistive Sensors Array

Sensors-29672-2019.R1

Strain Mapping Inkjet-Printed Resistive Sensors Array

M. A. Costa Angeli, F. Caronna, T. Cramer, D. Gastaldi, L. Magagnin, B. Fraboni, P. Vena

Abstract— **Inkjet printing is a promising low-cost fabrication technique capable of depositing functional materials with micrometer resolution, making this technique attractive for the fabrication of deformable sensors. Despite all the possible promising applications, no examples of inkjet-printed strain sensors array able to map substrate surface deformation have been proposed yet. On the base of these premises, it is here presented the development and characterization of an all-inkjet-printed resistive strain sensors array, highlighting the criteria adopted in the design phase. Initially, the strain sensing behavior of the printed CNTs percolation matrix was investigated by fabricating and electromechanically characterizing a single sensor. The proposed single sensor featured a sensitivity of 7.2 ± 2 up to 2.5% strain, demonstrating that the proposed sensing material is suitable for the fabrication of an inkjet-printed strain sensors array. Moreover, the fabricated sensors array was characterized through a confined electromechanical tensile test in which a non-homogeneous strain state was applied. Results showed the mapping capability of inkjet-printed deformable sensors array that is able to measure different local strains on the substrate surface. This work paves the way for using inkjet-printing technique for the realization of sensors with a larger number of interesting applications.**

***Index Terms*—Flexible electronics, inkjet-printing, sensors arrays, strain sensors.**

I. INTRODUCTION

Deformable electronics has the objective to develop sensing platforms able to conform to non-planar surface and to adapt to deformations. Research in deformable electronics has led to new fabrication methods that achieve deposition of layers of microstructured electronic materials on large-area plastic substrate. Among those methods, inkjet-printing has been established in extensive research work as a low-cost, rapid prototyping technique. Several deformable electronic circuits, such as MEMS, flexible antennas, physical and chemical sensors have been realized by inkjet-printing [1]–[4]. The success of this technology is related to its cheapness and easiness, as well as the possibility, contrary to the traditional fabrication methods, e.g. photolithography, to print on polymeric substrates with low softening temperature, such as polyethylene terephthalate (PET). Moreover, this technique has driven the exploration of a broad selection of ink formulations enabling the processing of diverse materials, including metals, conductive polymers, semiconductors, and insulators by printing. Inkjet-printing technology allows the deposition of functional materials incompatible with conventional manufacturing processes for electronics, like nanomaterials. Silver nanoparticles (AgNPs), silver nanowires (AgNWs) and carbon nanotubes (CNTs) can be dispersed in a liquid phase and directly printed on deformable substrates [5], [6]. Among them, AgNPs ink is a widely applied choice for developing inkjet-printed interconnects, due to its facile deposition and high electrical conductivity (10% of bulk Ag) [7]. In this context, the latest discoveries about materials and technologies for printed electronics have favored the growth of the deformable sensors field. Several printed sensors devices have been proposed in the literature. They employ distinct transduction mechanisms to convert chemical (e.g. pH, glucose), mechanical (e.g. strain, pressure) or optical signals into an electric one [8]–[12]. Printed low-cost resistive strain sensors have been reported to reach and even exceed the sensing performance of the traditional strain gauges [13]. Strain gauges transduce the mechanical deformation into a relative resistance variation, and its sensitivity is defined by the Gauge Factor, defined as $GF = \Delta R/(R_0\ \varepsilon)$. Traditional commercial strain gauges feature a sensitivity of 2 in a limited strain range, below 4% [14]. Therefore, many efforts have been made to improve both sensitivity and strain range of printed strain sensors [15], [16]. Even though many inkjet-printed resistive strain sensors featuring high performance were reported, few works are focus on the development and characterization of a sensors array [17]–[19]. The latter could be employed as a useful tool for the development of instrumented medical devices and surgical tools [20]. One interesting application could be the realization of instrumented balloon catheters able to provide feedback control to the surgeon [21]. Indeed, during inflation sensors array can map the applied strain on the balloon giving quantitative information on its condition. Flexible sensors arrays can also be coupled with orthopaedic implants in order to realize implantable therapeutic devices with diagnostic capabilities, known as smart implants [22]. Such devices, being capable to measure physical parameters from inside the body, such as pressure, temperature or strains, can open the way for the development of customized postoperative and rehabilitative treatments, also leading to implant design and surgical techniques improvement.

Despite all the possible promising applications, to the best of our knowledge, no examples of inkjet-printed strain sensors array able to map substrate surface deformation have been proposed yet. It is worthy of note that the development of strain mapping devices faces an additional challenge with respect to a

This article has been accepted for publication in a future issue of this journal, but has not been fully edited. Content may change prior to final publication. Citation information: DOI 10.1109/JSEN.2019.2961747, IEEE Sensors Journal

single sensor device. A sensor array should not only have a clear response to the applied deformation, but it should also be able to guarantee one-to-one correspondence between the measured resistance of each channel and the spatial localization of the physical stimulus. This is difficult to achieve as the response of each sensor in an array includes also the electromechanical contribution of interconnections (in series with the sensing material), which being bonded to the substrate are involved in stretching too. As a consequence, it is necessary to optimize the array design, sensor impedances and interconnects arrangement in order to minimize the impact of unavoidable resistance change of interconnects.

In this paper, a fully-inkjet-printed uniaxial strain mapping array is proposed, highlighting design requirements that must be considered in order to realize a strain sensor array. A multi-walled carbon nanotubes (CNTs) percolation matrix is proposed as sensing material. Ink concentration and layers number were optimized and, initially, the strain sensing behavior was investigated through the fabrication and electromechanical characterization of a single sensor. Results showed that the proposed sensor featured a GF of 7.2 ± 2 over a strain up to 2.5 %, which is higher than that measured for AgNPs interconnects. Then the design strategy and fabrication procedure of the sensor array are presented. The sensor array was characterized through a confined electromechanical tensile test applying both homogeneous and non-homogeneous strain states. The latter demonstrated the local strain mapping capability of the inkjet-printed sensor array.

II. Materials and Methods

A. *Inkjet-printing system*

In this study a research inkjet printer, Dimatix DMP-2850 (Fujifilm) equipped with a DMC-11610 cartridge was used to realize both single sensor and sensors array on a polymeric film (23 μm thick PET, GoodFellow). The printing system is based on 16 piezoelectric nozzles, with orifices size of 21.5 μm and 10 pL nominal drop volume.

B. *Inks*

A commercial silver nanoparticles ink (AgNPs, Silverjet DGP-40LT-15C, Advanced Nano Products) was used to print electrical connections; whereas multi-walled carbon nanotubes (CNTs) dispersion was formulated in order to realize a strain-sensing percolation matrix. Water was chosen as solvent because water-based ink is environmentally friendly, easy to store and less aggressive to the piezoelectric system than traditional organic solvents, thus enabling a longer cartridge lifetime. CNTs ink was obtained by dispersing 8 mg of commercial COOH functionalized CNTs (Merck) in 4 ml DI water (2 mg/ml) by means of probe sonicator, UP200Ht (Hielscher). The dispersion was cooled with ice to avoid overheating caused by the sonication process, which was performed at regular intervals of 1 minute followed by a 1-minute rest. The total sonication time was 5 minutes. However, CNTs tend to agglomerate in water due to the high Van der Waals mutual interaction forces which hinder their dispersion [23].

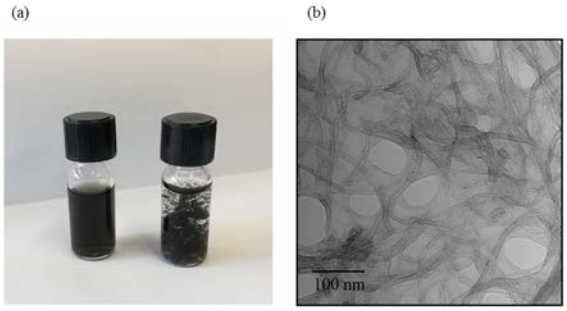

Fig.1 (a) Water-based CNTs dispersion with (left) and without (right) surfactant (Triton-X-100) 3h after sonication. It is clearly visible the formation of bulges in the latter one. (b) TEM image of the CNTs dispersion.

Dispersion, homogeneity and stability over time is an essential requirement of inkjet printing technique, hence it guarantees high printing quality, limiting nozzle clogging. Indeed, the latter is a struggling problem, especially when high aspect ratio nanomaterials, as CNTs, are used. As a rule of thumb, the nanoobject' s long size should be 1/100 of the nozzle diameter (21.5 μm) in order to limit clogging during printing. This criterion might not be as stringent for CNTs due to the possibility of flow-induced alignment as they passed through the nozzle. However, they are prone to be entangled and bundled [24]. Therefore, only stable and low-concentrated dispersion of small CNTs can be successfully printed. Based on these considerations thin and short COOH functionalized CNTs were employed, featuring nominal diameter and length of 9.5 nm and 1.5 μm, respectively. Carboxylation is a common type of sidewall functionalization through which carboxyl groups (-COOH) are chemically attached to nanotubes external walls. The presence of hydrophilic groups hinders nanotubes natural bundling promoted by sidewall hydrophobicity, thus favoring their dispersion [25]. However, we observed that the water dispersion of solely COOH-functionalized CNTs aggregates into bundles only 3 hours after the sonication process, as shown by visual observation in Fig. 1(a). Instead, adding a concentration of 0.1 (v/v) % of a surfactant, Triton X-100 (TX-100, Merck), is enough to assure a good dispersion for 1 month.

Moreover, the presence of surfactant not only leads to a more homogeneous and stabilized suspension, but also changes ink surface tension, thus improving its wettability. Indeed, static contact angles of the prepared CNTs inks with and without TritonX-100 were 31° ± 5° and 55° ± 4° on PET substrate, respectively. Such contact angle decrease enhances the wettability between the CNTs ink and substrate ensuring better ink printability and adhesion.

A TEM image of the CNTs dispersion is shown in Fig. 1(b), where surfactant that surrounds nanotubes is clearly visible. TritonX-100 is a non-ionic surfactant with a benzene ring tail, characterized by a decomposition temperature of 150 °C [26]. As a consequence, the sensor sintering temperature (100°C) it is too low to guarantee its decomposition, therefore we can assume that it remains around CNTs also after the sintering process, thus lowering the overall CNTs matrix electrical conductivity.

This article has been accepted for publication in a future issue of this journal, but has not been fully edited. Content may change prior to final publication. Citation information: DOI 10.1109/JSEN.2019.2961747, IEEE Sensors Journal

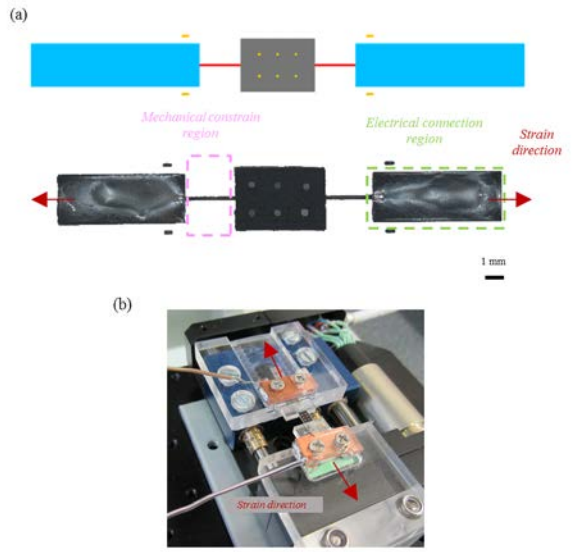

Fig.2 (a) Inkjet-printed single strain sensor on PET. Printed elements: (red) AgNPs interconnect, (yellow) AgNPs markers, (blue) AgNPs pads, (black) CNTs sensors. The sample was specifically designed for performing the electromechanical analysis of the sensing material (CNTs/EVA) only. (b) Electromechanical set up (in-house developed displacement driven micro-tensile machine) for the characterization of single sensor samples.

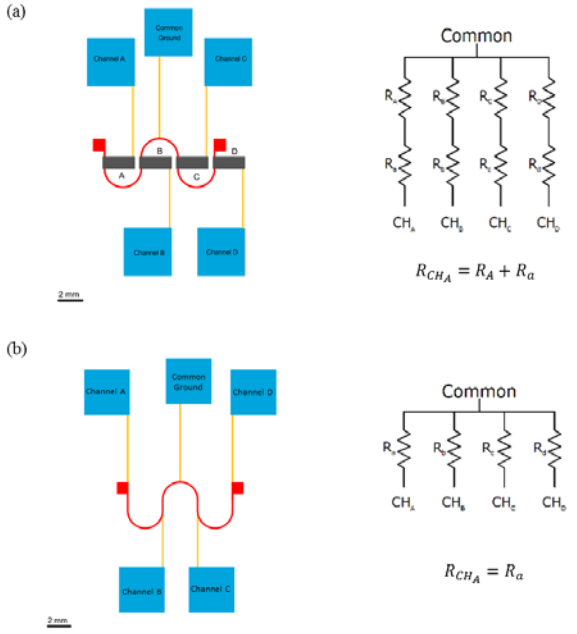

Fig.3 (a) (left) Uniaxial strain sensors array. Printing order: (red) AgNPs serpentine interconnect, (yellow) AgNPs linear interconnects, (blue) AgNPs pads, (black) CNTs sensors. (rigth) The electrical scheme of the array design, where capital letters (A B C D) are used for identifying each sensor (from left to right), and lowercase letters (a, b, c, d) are used for indicating silver interconnects resistance associated to each sensor. The measured resistance per each channel (i.e. channel A, RCHA) is the sum of sensor resistance (RA) and the resistance of the AgNPs components in series with sensor (Ra). (b) Scheme of the sample featuring the solely AgNPs interconnects of the sensors array. Printed elements: (red) AgNPs serpentine interconnect, (yellow) AgNPs linear interconnects, (blue) AgNPs pads. (right) The electrical model of the sample, the measured resistance per each channel (RCHA) is the resistance of the AgNPs components in series with sensor (Ra).

C. Fabrication

Before printing, the polymeric substrate was treated with an alkaline etching process, as previously reported [27], in order to improve ink adhesion. Both single and arrays sensors were fabricated by means of a multi-step process. Firstly, one layer of AgNPs ink was deposited using a 1 kHz frequency, 60°C substrate temperature and a drop spacing ranging between 30 and 45 µm depending on the pattern geometry. After cooling down the platen at room temperature (25-28 °C), CNTs dispersion was printed using a drop spacing of 10 µm and a frequency of 3 kHz. The entire pattern was annealed at 100 °C for 1h in order to evaporate the solvent and ensure good electrical conductivity. Finally, sensor encapsulation was performed by spin-coating a thin Ethylene Vinyl Acetate (EVA) layer on the entire printed pattern.

D. Single sensors

For the sensing material characterization, single sensors were realized. A rectangular sensing area of 2.5 × 3.5 mm^2 has been printed using the CNTs ink and AgNPs linear interconnections have been used, thus developing single strain sensors, as shown in Fig. 2(a). Six AgNPs equally spaced dots were printed on each sensor to be used as strain-markers for in-situ real strain evaluation. Sensor geometry was specifically designed for testing sensing area only, making sure that interconnections and electrical pads did not deform during the experiment, since only sensor resistance response under stretching should be analyzed, Fig. 2(b).

E. Sensors array

Fig. 3(a) shows the 4-sensors array geometry that was designed as uniaxial-strain mapping sensor. Interconnections arrangement was specifically designed for ensuring both current flows along straining direction and an electrically symmetric structure, hence sensors A and B have the same interconnects length of sensor C and D. A serpentine interconnect (red in Fig. 3(a)), placed along the strain direction, links all sensors together defining the common node. Straight lines (yellow in Fig. 3(a)), printed perpendicularly to the strain direction, connect each sensor to an AgNPs square 4 mm x 4 mm pad (blue in Fig. 3(a)), required for the electrical connection with the readout system. The sensor array is inscribed in a 45 mm x 45 mm square, marked at the four corners with reference points. These points were used to perform the alignment for multi-steps printing procedure, ensuring a good layer overlap. Moreover, specific lines and marks were printed in order to facilitate sample positioning on the testing machine.

A simplified electrical scheme of sensor array connections is presented in Fig. 3(a), where capital letters (A B C D) are used for identifying each sensor (from left to right), and lowercase letters (a, b, c, d) are used for indicating silver interconnects resistance associated to each sensor. As the electrical scheme highlights, interconnection resistances are in series with sensing materials, and the overall resistance (e.g. channel A) measured by the external unit is R_{CH_A}=R_a+R_A. The response of each sensor (R_{CH}) includes the electromechanical contribution of printed AgNPs elements (R_a), which are involved in stretching too. Indeed, when a deformation (ε) is

This article has been accepted for publication in a future issue of this journal, but has not been fully edited. Content may change prior to final publication. Citation information: DOI 10.1109/JSEN.2019.2961747, IEEE Sensors Journal

applied, the measured resistance becomes $R_{CH_A}(\varepsilon)=R_a+\Delta R_a+R_A+\Delta R_A$, where ΔR_A is the resistance variation of the sensing element, and ΔR_a is the resistance variation of the AgNPs components in series with sensor A. Therefore, a negligible effect of interconnects is required in order to guarantee a one-to-one correspondence between the measured resistance by each channel and the spatial localization of the deformation on each sensor. This is ensured only if both following conditions are fulfilled: $\Delta R_A > \Delta R_a$ and $R_A > R_a$. It is worth noting that these are requirements strictly correlated to the design of a strain mapping array and they are not necessary for the design of a single sensor.

Fig.3(b) shows a sample composed of solely AgNPs interconnects of sensors array. This latter sample has been manufactured by printing the AgNPs skeleton having the same geometry of the sample in Fig. 3(a); while sensors were not printed. This sample was designed in order to compare, per each channel, the resistance variation of the solely AgNPs components (ΔR_a) with the measured channel response, $R_{CH_A}(\varepsilon)$, which includes both the sensor (ΔR_A) and series resistance (ΔR_a) change.

A multi-step process was performed in order to fabricate the sensors array. Indeed, inkjet printing is a versatile fabrication method that allows obtaining accurate alignment with patterns already present on the substrate, which is an indispensable function for patterning multi-layered devices with different materials. However, inkjet-printed patterns are always characterized by defects, such as voids and bulges, that are the result of surface imperfections or misaligned jets and clogged nozzles. The probability of this phenomenon increases with increasing complexity and dimension of the printed area. Moreover, the printing quality is strongly affected by the sample geometry and printing direction [27]. Therefore, the array manufacturing requires printing four different layers. These are firstly related to the use of different materials, secondly to the printing of several geometries requiring specific printing directions and parameters. Moreover, the multi-steps fabrication process allows the early detection of eventual defects in the printing structure, which could hinder device functioning and performance, and ensures a higher quality of the printed pattern. Therefore, serpentine interconnect was printed as first layer, being the most complex and difficult to print geometry of the pattern, followed by linear interconnects, square pads and the four CNTs sensors. The latter were printed all together in order to guarantee good inter-sensors repeatability.

F. Electromechanical tests

Samples mechanical straining has been performed using two different miniaturized in-house developed displacement driven micro-tensile machines for single and array samples. As concern single strain sensors, a 1 μm/s displacement rate was set for all tests, employing a ramp strain history, and resistance was recorded in real-time using Keithley 3706 System Multimeter by means of a two-probing method. These tests were coupled with an in-situ observation using a confocal laser microscope (Olympus LEXT OLS4100). An image stack flow was recorded every 1% nominal strain, enough to detect the displacement with the microscope resolution.

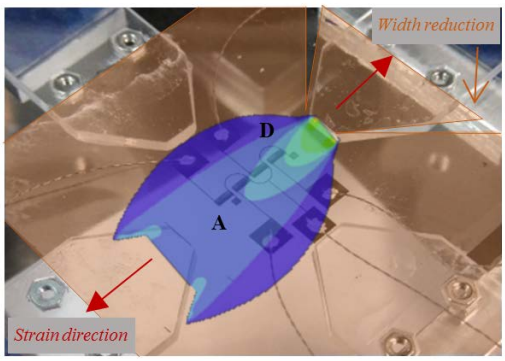

Fig.4 Electromechanical set up for array characterization in the case of non-homogeneous deformation. PET substrate (yellow square) was cut near sensors D in order to reduce the substrate width. A colour map of the expected non-homogeneous strain field is superimposed: sensor D is subjected to higher local strain than that of sensor A. The qualitative colour map was obtained through a preliminary finite element simulation.

In the case of the sensor array, electromechanical confined tensile tests applying different strain histories were performed. PET substrate was cut as a square of 45 mm x 45 mm and mounted on the testing device by means of specific appropriate procedures for sample alignment and assembling. A data acquisition system has been designed and implemented to allow the measurement of all sensors simultaneously through a multichannel system. Sensor cables were connected to a multiplexer (Mux-Board, Quad SPDT Switch ADG333A, Analog Devices) controlled by a Keysight Source Unit of measurement that was used in order allow fast switching (0.6 s) between channels. During measurements, the readout current-voltage characteristics were transferred to the computer and graphically visualized. Constant strain rate ramp tests and increasing loading-partial unloading strain histories were performed applying a 5 μm/s displacement rate. In loading-partial unloading tests each loading phase of 1% net strain is followed by an unloading phase of half of its amount (0.5% strain recovered). As a result, each loading series corresponds to an actual increment of 0.5% nominal strain. Elongation strain was applied along the direction of the sensor alignment; while, along the direction perpendicular to the load direction, transverse contraction was confined. This lateral confinement is needed in order to avoid wrinkles forming on uniaxially loaded thin sheet.

Moreover, heterogeneous deformation states were applied to the substrate in order to investigate the strain-mapping capability of the device. A strain gradient was applied by reducing the transverse width of the polymer substrate on one of the loading sides. It was reduced by cutting the substrate near sensor D, as shown in Fig. 4. In this way, the four sensors were subjected to a tensile strain whose amplitude increases from sensor A (less stretched) to sensors D (most stretched), as qualitatively shown in the color strain map in Fig. 4.

III. RESULTS AND DISCUSSION

This article has been accepted for publication in a future issue of this journal, but has not been fully edited. Content may change prior to final publication. Citation information: DOI 10.1109/JSEN.2019.2961747, IEEE Sensors Journal

A. CNTs percolation network

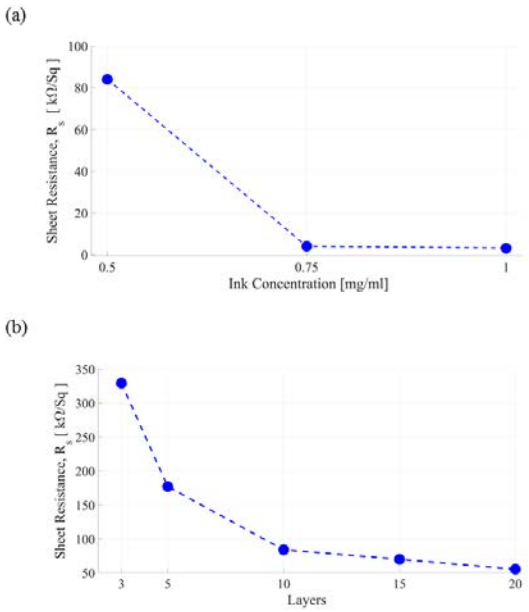

Fig.5 (a) CNTs sheet resistance as function of CNTs ink concentration. (b) CNTs sheet resistance as function of printed layers for 0.5 mg/ml ink.

CNTs arrangement and thus sensor sensitivity are related to both ink concentration and number of layers. Indeed strain-sensitivity of a percolation matrix is strictly correlated to filler concentration: GF value increases decreasing CNTs loading and reaches its highest value around the percolation threshold [28], [29]. The percolation threshold is the volume fraction of filler where an abrupt change of conductivity is observed. Since it is difficult defining the thickness of inkjet-printed structures, sheet resistance was used instead of conductivity. Therefore, sheet resistance was evaluated as function of CNTs ink concentration and printed layers number in order to define the optimum printing parameters for the sensing area manufacturing. Several samples have been printed changing both CNTs concentration and overwriting steps, ranging from 0.25 to 1 mg/ml and from 3 to 20 layers. As expected, the network resistance decreases as both CNTs concentration and number of layers increases, as shown in Fig.5(a) and 5(b), respectively. It is worth noting that these two parameters are mutually dependent, and their choice is limited by the fabrication process and the properties of the read-out instrument. Considering layers number, the minimum value necessary to obtain a uniformly distributed sensing area was found to be equal to ten. Samples fabricated using less than ten layers featured, through optical observation, non-homogeneous CNTs distribution. This phenomenon can be ascribed to the microfluidic flow generated during solvent evaporation. Only after ten layers (regardless of ink concentration) the printed region exhibited acceptable uniformity. AFM analysis carried out on 10 layers of 0.5 mg/ml CNTs dispersion inkjet printed on PET substrate Fig. 6, shows that CNTs are uniformly distributed and randomly organized on the entire area, providing a homogeneous percolation network.

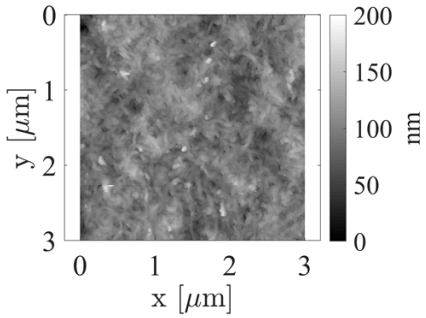

Fig.6 AFM image of 10 layers of 0.5 mg/ml CNTs dispersion inkjet printed on PET substrate.

On the contrary, for what concerns ink concentration, an upper limit is set by the fabrication process, indeed above 1 mg/mL, printing was impossible due to nozzles clogging.

Moreover, we can also define a lower limit that is imposed by the measurable resistance. Indeed, the minimum concentration for which samples showed electrical conductivity turned out to be 0.5 mg/ml, since samples printed with a 0.25 mg/ml ink exhibited resistance values overcoming the measuring instrument upper limit (120 MΩ).

Based on these considerations, 10 layers of 0.5 mg/ml concentrated CNTs dispersion was chosen as the most suitable layers number/concentration pair to be used for sensing area manufacturing.

B. Single sensors

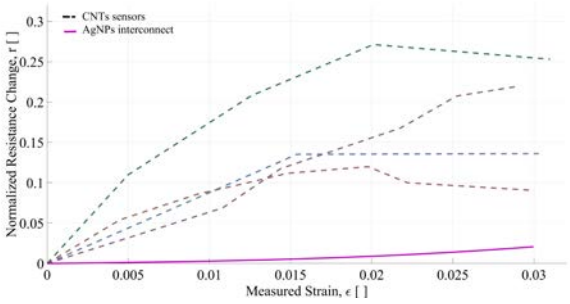

Fig.7 Normalized Resisnace change (r=R-R0/R0) of four single CNTs/EVA strain sensors (dashed line) and one AgNPs interconnects sample (solid line).

Fig. 7 shows the electromechanical response ($r = R-R_0/R_0$) of four samples of EVA covered CNTs single sensors. Curves showed similar behavior with resistance increasing trend up to 2.5 % strain, with an average GF of 7.2 ± 2. Considering a similar strain range, the achieved strain sensing performance exhibits a good sensitivity if compared with inkjet-printed sensors reported in previous works found in the literature [16]–[19]. However, in order to develop the sensors array the sensing material performance takes relevance only if compared with the electrical and electromechanical behavior of the material used to realize interconnects, in this case AgNPs ink. Thus, its electromechanical behavior has been compared with previously presented results on inkjet-printed serpentine-

shape AgNPs interconnects [27]. Therefore, comparing their electromechanical behavior in the strain range of interest (up to 2.5% strain) the sensing material featured a GF 10 times higher than AgNPs interconnects. Moreover, sheet resistance of sensing material (10.4 ± 0.9 kΩ/Sq) and silver interconnects (1.7± 0.3 Ω/Sq) differ by three orders of magnitude. On this basis, it could be concluded that the proposed CNTs/EVA pair is a suitable sensing material for sensors array fabrication.

C. *Strain sensors array*

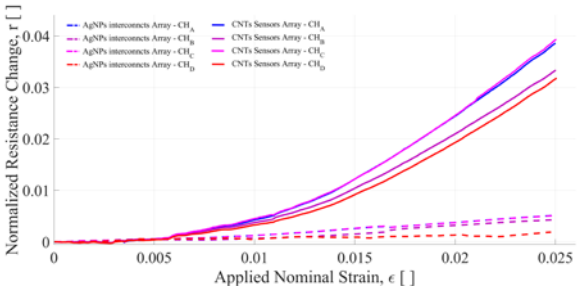

Fig.8 Normalized resistance change for each channel (A, B, C, D) of the sensors array (i.e channel A, RCHA (ε)=Ra+ ΔRa+ RA+ΔRA, solid line) and the solely AgNPs interconnects (RCHA(ε)= Ra+ ΔRa, dashed line) imposing a ramp strain history up to 2.5% in confined condition.

Initially, the electromechanical response of the sample featuring the solely AgNPs components (serpentine interconnect, straight lines and pads, $R_{CH_A}(\varepsilon)=R_a+\Delta R_a$) of the array, Fig. 3(b), was compared with the sensors array, Fig. 3(a), behaviour ($R_{CH_A}(\varepsilon)=R_a+\Delta R_a+R_A+\Delta R_A$) performing a ramp test up to 2.5 % nominal strain. The electromechanical contribution of AgNPs interconnects is negligible since R_a is only 1% of the entire patch sensor resistance (150 ± 40 Ω of about 20.8 ± 3 kΩ) and a very small interconnects resistance variation ΔR_a occurs under stretching, as shown in Fig. 8. As a consequence, AgNPs interconnections influence was not considered, and sensors electromechanical response was ascribed to the sensing area only. Indeed, the error caused by this approximation is less than 0.5% of the array response.

The response of the sensors array subjected to the homogeneous strain field is presented in Fig. 9. The four sensors showed a similar behavior that proves that they featured comparable sensitivity. Indeed, the difference between the normalized resistances of the two external sensors (D and A), shown in Fig. 9(b), is less than 0.006, i.e. 13% of sensor response, which is attributable to the response variability between different sensors of the same array. However, the difference between the normalized resistances of the two external sensors D and A (solid line in Figure 9(b)) increased with the applied strain. This discrepancy is related to the fact that, despite a homogenous deformation was applied, sensors may be subjected to a slightly different local strain and this mismatch may increase over time due to time drift of the whole system. This drifting response was characterized by performing a suitably designed experiment as discussed below.

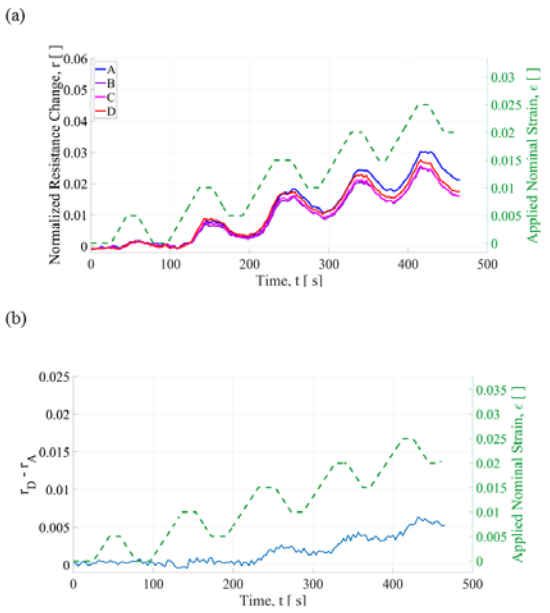

Fig.9 (a) Normalized resistance vs time of each sensor (A-D) in customized loading-unloading experiments in the homogeneous configuration. (b) Normalized resistance difference (rD-rA) of the two external sensors (D and A) vs time. The applied nominal strain history (dashed line) is also shown in the same plots.

All sensors showed a clear response at each strain step, with a detection limit of 0.5% nominal strain. The four sensors exhibited a reversible resistance behaviour, since resistance recovery occurred after each unloading step, although a sensor lag, owed to the viscous response of the polymeric substrate, was observed. This specific effect related to the mechanical behaviour of the polymers used as substrate and as capping layer needs further investigations. The specific resistance change versus strain for the sensor array was lower respect to the single sensor. This difference is related to the different deformation mechanisms applied to the array if compared to that applied to the single sensors. Single senor was characterized through a tensile test with free transverse contraction, whereas array sensors were characterized through a confined lateral contraction. This specific deformation mode is mainly motivated by the application envisaged for the devices.

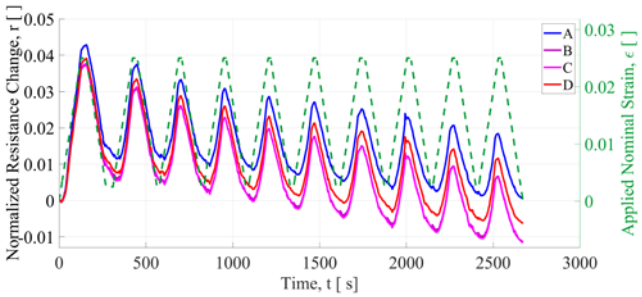

Fig. 10 Cyclic electromechanical behaviour of sensors array imposing a 2.5% maximum nominal strain (dashed line).

This article has been accepted for publication in a future issue of this journal, but has not been fully edited. Content may change prior to final publication. Citation information: DOI 10.1109/JSEN.2019.2961747, IEEE Sensors Journal

The sensors array was tested applying cyclic strain history. This experiment was aimed at discussing the drifting behavior and repeatability of the manufactured sensors array. The sample was loaded up to a 2.5% axial deformation and partial unloading, repeating this procedure ten times. The lower boundary of the strain cycles was 0.25%, this value was selected with the purpose to avoid sample buckling upon compression due to plastic (or creep) strain occurring in the polymer substrate. Resistance change in the first loading cycle is in alignment with that obtained through the ramp test, Fig. 8. However, only partial resistance recovery occurred after each cycle. Moreover, sensors showed a drift that is related to the time-dependent mechanical response of the polymer used as a substrate. Indeed, PET substrate features viscous-elastic mechanical behavior with a limited elastic range that hinder to be used for multiple usages.

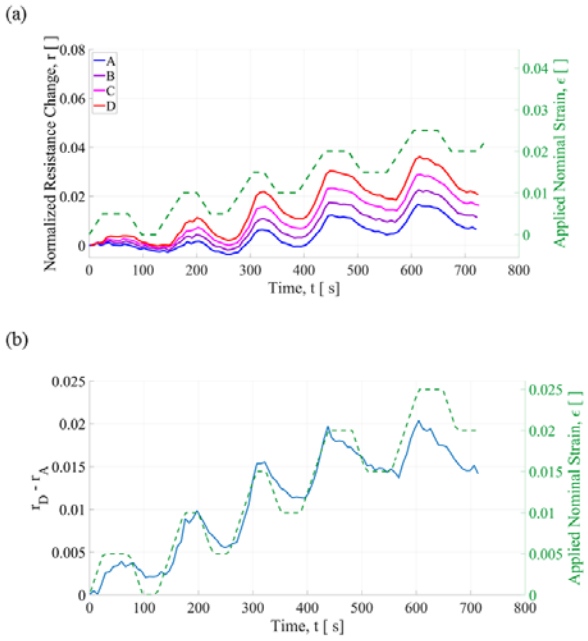

Fig. 11 (a) Normalized resistance vs time of each sensor (A-D) in customized loading-unloading experiments in non-homogeneous configuration. (b) Normalized resistance difference (rD-rA) of the two external sensors (D and A) vs time for the non-homogenous configuration (sensor D is the most strained). The applied nominal strain history (dashed line) is also shown in the same plots.

In the non-homogeneous straining, as shown in Fig. 11 (a), sensors showed a different response (in amplitude) that it is consistent with the different strain applied: sensor D showed the highest resistance change and the electromechanical response decreases from sensors D to A, accordingly to the applied local strain. Indeed, sensor D features a resistance variation 3 times higher than sensor A and so the difference between the normalized resistances of the two external sensors (r_D-r_A), Fig. 11(b), is mainly related to differences in local strains rather than intrinsic sensor response variability consequent to the printing process. In conclusion, this simple testing procedure has proved that the proposed strain sensors array is able to measure the local strain applied to the substrate.

IV. Conclusions

In this paper, a fully inkjet-printed uniaxial strain sensors array is presented. Firstly, the strain-sensing capability of the CNTs matrix was experimentally characterized through electromechanical uniaxial tensile tests on single sensors. The average gauge factor of CNTs printed sensor was 7.2 ± 2. which is higher than commercial strain gauge (limited to 2), and in the range of GFs found for inkjet-printed strain sensors in literature [19], [30], [31]. However, sensors showed limited linearity up to 2.5% strain that set the maximum sensor's sensing range. This value is lower than commercial strain gauge (around 4%), but considering similar substrates and fabrication technique, it is in the literature range [14], [18], [19], [32] and it is consistent with the linear elastic range of the substrate (around 3% strain). This sensor's feature could be improved by performing a further study on a suitable selection of materials (i.e elastomeric substrata).

Inkjet-printing was used to fabricate the sensors array, demonstrating that this is a technology suitable for the production of layered structures characterized by complex geometries and made by different materials. Firstly, we proved that the array design guarantees a one-to-one correspondence between the measured resistance of each channel and the spatial localization of the local deformation because the electromechanical response of array interconnects is negligible. Sensors array showed a different, lower and non-linear, electromechanical performance to respect single sensors. This behavior is related to the different deformation mechanisms: single senor was characterized through a tensile test with free transverse contraction, whereas array sensors were characterized through a confined lateral contraction. Thus, this result showed as the absence of the free transverse contraction of the substrate modifies the CNTs response to the stretching. The sensors array is meant to be applied on a planar surface and thus deform accordingly. Planar surfaces are subjected, in the simplest case, to a biaxial strain state. Therefore, the confined tensile test can better mimic a real application for strain sensors array rather than a free transverse contraction loading scheme. An additional motivation for introducing the lateral constraint on the patch with the sensor array is related to the geometry of the patch itself. Having the patch a rectangular shape with similar size in the two dimensions, the application of a tensile load in one direction would produce wrinkles in the transverse direction if no mechanical constraint is provided. The wrinkles would have affected the sensor response invalidating its read-out. Future analysis should be aimed to properly characterize this particular behavior.

The drifting behaviour shown by the sensor array and potential irreversible residual strain in the polymeric substrate may limit the application of this kind of devices. Further study on material selection for the substrate is needed in order to improve this specific aspect.

Sensors array electromechanical reaction to the application of non-homogeneous strain field was measured. Although the simplicity of such testing procedure, the results showed the mapping capability of the inkjet-printed sensor array, which is able to detect different local strains on the same surface. Since the proposed array has proved that can be successfully employed as strain mapping sensor, further

experiments aimed to properly quantify the spatial resolution should be performed.

REFERENCES

[1] J. Byun *et al.*, "Fully printable, strain-engineered electronic wrap for customizable soft electronics," *Sci. Rep.*, vol. 7, no. February, pp. 1–11, 2017.

[2] M. A. U. Karim, S. Chung, E. Alon, and V. Subramanian, "Fully Inkjet-Printed Stress-Tolerant Microelectromechanical Reed Relays for Large-Area Electronics," *Adv. Electron. Mater.*, vol. 2, no. 5, pp. 1–8, 2016.

[3] Y. Liu and E. Devices, "M Ultifunctional C Arbon N Anotube S Ensors for E Nvironmental M Onitoring," *4th World Conf. Struct. Control Monit.*, no. March, pp. 1–8, 2012.

[4] S. Kim, A. Georgiadis, and M. M. Tentzeris, "Design of inkjet-printed RFID-based sensor on paper: Single- and dual-tag sensor topologies," *Sensors (Switzerland)*, vol. 18, no. 6, pp. 1–11, 2018.

[5] A. Denneulin, J. Bras, F. Carcone, C. Neuman, and A. Blayo, "Impact of ink formulation on carbon nanotube network organization within inkjet printed conductive films," *Carbon N. Y.*, vol. 49, no. 8, pp. 2603–2614, 2011.

[6] D. J. Finn, M. Lotya, and J. N. Coleman, "Inkjet printing of silver nanowire networks," *ACS Appl. Mater. Interfaces*, vol. 7, no. 17, pp. 9254–9261, 2015.

[7] H. H. Lee, K. Sen Chou, and K. C. Huang, "Inkjet printing of nanosized silver colloids," *Nanotechnology*, vol. 16, no. 10, pp. 2436–2441, 2005.

[8] M. Borghetti, M. Serpelloni, E. Sardini, and S. Pandini, "Mechanical behavior of strain sensors based on PEDOT:PSS and silver nanoparticles inks deposited on polymer substrate by inkjet printing," *Sensors Actuators, A Phys.*, vol. 243, pp. 71–80, 2016.

[9] K. S. Bhat, R. Ahmad, J. Y. Yoo, and Y. B. Hahn, "Fully nozzle-jet printed non-enzymatic electrode for biosensing application," *J. Colloid Interface Sci.*, vol. 512, pp. 480–488, 2018.

[10] L. Basiricò, P. Cosseddu, A. Bonfiglio, R. Neelgund, and H. W. Tyrer, "Inkjet printed arrays of pressure sensors based on all-organic field effect transistors," *2010 Annu. Int. Conf. IEEE Eng. Med. Biol. Soc. EMBC'10*, pp. 2111–2114, 2010.

[11] G. L. Goh, S. Agarwala, Y. J. Tan, and W. Y. Yeong, "A low cost and flexible carbon nanotube pH sensor fabricated using aerosol jet technology for live cell applications," *Sensors Actuators, B Chem.*, vol. 260, pp. 227–235, 2018.

[12] Y. Khan *et al.*, "Inkjet-Printed Flexible Gold Electrode Arrays for Bioelectronic Interfaces," *Adv. Funct. Mater.*, vol. 26, no. 7, pp. 1004–1013, 2016.

[13] S. Cruz, D. Dias, J. C. Viana, and L. A. Rocha, "Inkjet Printed Pressure Sensing Platform for Postural Imbalance Monitoring," *IEEE Trans. Instrum. Meas.*, vol. 64, no. 10, pp. 2813–2820, 2015.

[14] O. Kravchuk and M. Reichenberger, "Properties and long-term behavior of nanoparticle based inkjet printed strain gauges," *J. Mater. Sci. Mater. Electron.*, vol. 27, no. 10, pp. 10934–10940, 2016.

[15] O. Kanoun *et al.*, "Flexible carbon nanotube films for high performance strain sensors," *Sensors (Switzerland)*, vol. 14, no. 6, pp. 10042–10071, 2014.

[16] Y. Zhang, N. Anderson, S. Bland, S. Nutt, G. Jursich, and S. Joshi, "All-printed strain sensors: Building blocks of the aircraft structural health monitoring system," *Sensors Actuators, A Phys.*, vol. 253, pp. 165–172, 2017.

[17] S. Fu *et al.*, "Fabrication of Large-Area Bimodal Sensors by All-Inkjet-Printing," *Adv. Mater. Technol.*, vol. 4, no. 4, pp. 1–9, 2019.

[18] F. Michelis, L. Bodelot, Y. Bonnassieux, and B. Lebental, "Highly reproducible, hysteresis-free, flexible strain sensors by inkjet printing of carbon nanotubes," *Carbon N. Y.*, vol. 95, pp. 1020–1026, 2015.

[19] V. Correia, C. Caparros, C. Casellas, L. Francesch, J. G. Rocha, and S. Lanceros-Mendez, "Development of inkjet printed strain sensors," *Smart Mater. Struct.*, vol. 22, no. 10, pp. 105028–105038, 2013.

[20] L. Klinker *et al.*, "Balloon catheters with integrated stretchable electronics for electrical stimulation, ablation and blood flow monitoring," *Extrem. Mech. Lett.*, vol. 3, pp. 45–54, 2015.

[21] D. H. Kim *et al.*, "Materials for multifunctional balloon catheters with capabilities in cardiac electrophysiological mapping and ablation therapy," *Nat. Mater.*, vol. 10, no. 4, pp. 316–323, 2011.

[22] E. H. Ledet, B. Liddle, K. Kradinova, and S. Harper, "Smart implants in orthopedic surgery, improving patient outcomes: a review," *Innov Entrep Heal.*, vol. 5, pp. 41–51, 2018.

[23] N. T. Dinh *et al.*, "High-resolution inkjet printing of conductive carbon nanotube twin lines utilizing evaporation-driven self-assembly," *Carbon N. Y.*, vol. 96, pp. 382–393, 2016.

[24] S. Kholghi Eshkalak, A. Chinnappan, W. A. D. M. Jayathilaka, M. Khatibzadeh, E. Kowsari, and S. Ramakrishna, "A review on inkjet printing of CNT composites for smart applications," *Appl. Mater. Today*, vol. 9, pp. 372–386, 2017.

[25] J. Lee, M. Kim, C. K. Hong, and S. E. Shim, "Measurement of the dispersion stability of pristine and surface-modified multiwalled carbon nanotubes in various nonpolar and polar solvents," *Meas. Sci. Technol.*, vol. 18, no. 12, pp. 3707–3712, 2007.

[26] K. Mitsuda, H. Kimura, and T. Murahashi, "Evaporation and decomposition of Triton X-100 under various gases and temperatures," *J. Mater. Sci.*, vol. 24, no. 2, pp. 413–419, 1989.

[27] M. A. Costa Angeli, T. Cramer, B. Fraboni, L. Magagnin, D. Gastaldi, and P. Vena, "Reliability of inkjet printed silver nanoparticle interconnects on deformable substrates tested through an electromechanical in-situ technique," *MRS Commun.*, vol. 9, no. 1, pp. 129–136, 2019.

[28] Alamusi, N. Hu, H. Fukunaga, S. Atobe, Y. Liu, and J. Li, "Piezoresistive strain sensors made from carbon

nanotubes based polymer nanocomposites," *Sensors*, vol. 11, no. 11, pp. 10691–10723, 2011.

[29] K. J. Loh, J. P. Lynch, B. S. Shim, and N. A. Kotov, "Tailoring piezoresistive sensitivity of multilayer carbon nanotube composite strain sensors," *J. Intell. Mater. Syst. Struct.*, vol. 19, no. 7, pp. 747–764, 2008.

[30] M. Borghetti, M. Serpelloni, E. Sardini, and S. Pandini, "Mechanical behavior of strain sensors based on PEDOT:PSS and silver nanoparticles inks deposited on polymer substrate by inkjet printing," *Sensors Actuators, A Phys.*, vol. 243, pp. 71–80, 2016.

[31] D. Ryu, F. N. Meyers, and K. J. Loh, "Inkjet-printed, flexible, and photoactive thin film strain sensors," *J. Intell. Mater. Syst. Struct.*, vol. 26, no. 13, pp. 1699–1710, 2015.

[32] B. Thompson and H. Yoon, "Aerosol-printed strain sensor using PEDOT:PSS," *IEEE Sens. J.*, vol. 13, no. 11, pp. 4256–4263, 2013.